Journal of Power Sources 196 (2011) 7097–7103

Contents lists available at ScienceDirect

Journal of Power Sources

journal homepage: www.elsevier.com/locate/jpowsour

Segmented cell testing for cathode parameter investigation

Pietro Tanasini[a,b,*], J. Andreas Schuler[a,c], Zacharie Wuillemin[a], Myriam L. Ben Ameur[a,b], Christos Comninellis[b], Jan Van herle[a]

[a] Industrial Energy Systems Laboratory (LENI), École Polytechnique Fédérale de Lausanne (EPFL), CH-1015 Lausanne, Switzerland
[b] Group of Electrochemical Engineering (GGEC), École Polytechnique Fédérale de Lausanne (EPFL), CH-1015 Lausanne, Switzerland
[c] Interdisciplinary Centre of Electron Microscopy (CIME), École Polytechnique Fédérale de Lausanne (EPFL), CH-1015 Lausanne, Switzerland

ARTICLE INFO

Article history:
Received 8 June 2010
Received in revised form 16 July 2010
Accepted 5 August 2010
Available online 17 August 2010

Keywords:
Segmented testing
SOFC
Cathode degradation
Long-term testing
Parallel testing

ABSTRACT

The increasing quality and durability of solid oxide fuel cells (SOFCs) state-of-the-art materials renders the long-term testing of fuel cells difficult since considerably long equipment times are needed to obtain valuable results. Moreover, reproducibility issues are common due to the high sensitivity of the performance and degradation on the testing conditions. An original segmented cell configuration has been adopted in order to carry out four tests in parallel, thus decreasing the total experimental time and ensuring the same operating conditions for the four segments. The investigation has been performed on both anode-supported cells and symmetrical Lanthanum-Strontium Manganite–Yttria-stabilized Zirconia (LSM–YSZ) electrolyte-supported cells. In separate tests, the influence of variables like cathode thickness, current density and cathode composition on performance and degradation have been explored on anode-supported cells. Furthermore, the effect of chromium poisoning has been studied on electrolyte-supported symmetric cells by contacting one segment with a chromium-iron interconnect material. Long-term polarization of the segments is controlled with a multi-channel galvanostatic device designed in-house. Electrochemical characterization has been performed through electrochemical impedance spectroscopy (EIS) at different H_2 partial pressures, temperatures and bias current, effectively demonstrating the direct impact of each studied variable on the cell performance and degradation behavior. Segmented cell testing has been proven to be an effective strategy to achieve better reproducibility for SOFC measurements since it avoids the inevitable fluctuations found in a series of successively run tests. Moreover, simultaneous testing increased *n*-fold the data output per experiment, implying a considerable economy of time.

1. Introduction

Solid oxide fuel cells (SOFCs) continue to be intensively studied as promising devices to convert high energy electrical with high efficiency. SOFCs are medium- or high-temperature fuel cells (600–900 °C) constituted by ceramic or cermet electrodes separated by an ion-conducting ceramic membrane. Their high operation temperature allows numerous fuels to be converted into electrical power and heat; moreover, as kinetics is relatively fast, the use of expensive noble metals as electrode catalysts is avoided. However, the harsh cell operation conditions have the downside of introducing deactivation processes that cause a decrease in performance and conversion efficiency. Several degradation phenomena have been studied, among others: (i) microstructural changes that reduce the active area and the conduction properties of the electrodes [1–5], (ii) solid state interfacial reactions between cell components and materials, leading to the formation of resistive phases [6–9], (iii) electrode poisoning by volatile, inorganic species (e.g. chromium [10–14]) blocking active sites and (iv) conductivity degradation of the ceramic electrolyte upon aging [15–17].

As SOFC life-time is a key factor for introduction into the market, several solutions have been found in the last years to hinder deactivation processes while maintaining or even increasing performance. From a materials point of view, the quality of the raw materials has been improved to limit the segregation of impurities, and the catalyst electrodes as well as their compositions have been selected to hinder the formation of foreign phases. From the technical point of view, system components, like metallic interconnectors or heat exchangers, have been chosen or treated to limit the emission of pollutants. Furthermore, operating conditions (e.g. temperature, fuel utilisation, cell overpotential) are optimized to limit degradation. Nevertheless, degradation phenomena are hindered, albeit not eliminated; thus, life-time is still an issue from an industrial point of view.

* Corresponding author at: GGEC-ISIC-SB, Station 6, EPFL, CH-1015 Lausanne, Switzerland. Tel.: +41 21 693 6189; fax: +41 21 693 3502.
E-mail addresses: pietro.tanasini@epfl.ch, pietrotanasini@tanarch.it (P. Tanasini).

0378-7753/$ – see front matter © 2010 Elsevier B.V. All rights reserved.
doi:10.1016/j.jpowsour.2010.08.034

As a consequence of the recent improvements allowing to achieve performance losses as low as 1% over 1000 h of continuous operation, the study of slow, simultaneous, interrelated degradation mechanisms is difficult due to the long testing time needed to measure significant variations in performance; further, the separation and quantification of the contributions of each phenomenon is even more challenging. Furthermore, degradation studies need robust and stable test benches permitting to identify changes of the order of 1% after months of aging. Operating conditions must be rigorously the same for all the tests of an experimental campaign, since even small changes in temperature or gas distribution affect the cell behavior and overrun the influence of a given studied variable. Reproducibility and testing time are key issues in state-of-the-art SOFC research.

The present work proposes an original testing strategy aiming on the one hand to reduce the time needed for an experimental campaign and, on the other hand, to ensure reproducibility of operating conditions. These two objectives are achieved by the so-called segmentation of a cell, allowing parallel simultaneous testing of each segment under the same operating conditions. Cell segmentation in our work is performed by depositing four separated cathodes either on an electrolyte-covered anode or, in a symmetrical configuration, on both sides of an electrolyte support. In both cases the measurements have been conducted independently on each segment, leading to the investigation of the effect of one specific variable (cathode thickness, current density, etc.) on the performance and aging behavior of the multi-cathode cell.

2. Experimental

2.1. Cell preparation

Two types of supports have been used: electrolyte-covered anode supports (AS) and electrolyte supports (ES) (Fig. 1). The 250 μm thick anode-supported half cells were manufactured by tape casting (HTceramix SA, Switzerland) using 55 wt% NiO and 45 wt% Yttria-stabilized Zirconia and co-sintering with a 5 μm thick 8% Yttria-stabilized Zirconia (8YSZ) electrolyte. The anode supports were then laser-cut to the shape of 60 mm discs; this allowed avoiding curved edges. The electrolyte supports were made of 3% Yttria-stabilized Zirconia (3YSZ) (Kerafol, Germany) as 82 mm-sided squares with a thickness of 115 μm.

All the other cell active layers were deposited by screen-printing and were made of Lanthanum-Strontium Manganite (LSM) of different compositions and 8YSZ with a volume ratio of 50/50. The composite powder was prepared mixing the as-received LSM and YSZ with ethanol in a ball-mill for 24 h in presence of zirconia spheres. Inks were printed layer by layer through stainless steel mesh on the anode-supported half cells. The inks were obtained mixing the powders on an alumina triple-roll mill with 3.2% ethylcellulose in terpineol as a binder (ratio powder/binder around 1.36).

Three experiments done on anode supports and one on electrolyte support will be illustrated in this publication.

The test A on anode support (AS-A) was aimed to investigate the effect of the current density on the cell operation; therefore four identical cathodes were deposited on the anode support. The materials used for the cathode inks were as received LSM $(La_{0.75}Sr_{025})_{0.90}MnO_{3\pm\delta}$ from Praxair, USA (LSM25) and 8YSZ (Tosoh Corp., Japan) both with a nominal average particle diameter of 0.5 μm. The cell was then sintered at 1100 °C for 1 h. The cathodes, covered with a LSM25 current collection layer, were contacted with platinum meshes.

The test B on anode support (AS-B) was aimed to investigate the effect of cathode thickness on cell operation; therefore four cathodes of identical composition were deposited on the anode support by screen-printing successively a different numbers of layers. Each layer consisted of approximately 5 μm of cathode material. The composition of the as received cathode material (Fuel Cells Materials, USA) was $(La_{0.70}Sr_{0.30})_{0.90}MnO_{3\pm\delta}$ (LSM30) with an average particle diameter equal to 0.3 μm and grinded 8YSZ (Tosoh Corp., Japan). Grinding was necessary in order to bring the average YSZ particle diameter down from 0.5 to 0.3 μm, so as to have the ratio between the particle diameters of the two phases close to the unity, which is a key parameter for percolation [18]. All particle size distributions and average particle diameters (d_{50}) have been measured by laser diffraction on a Mastersizer (Malvern Instrument, UK). The cell was then sintered at 1050 °C for 1 h. The cathodes, covered with a $(La_{0.65}Sr_{0.35})_{0.95}MnO_{3\pm\delta}$ (LSM35, Fuel Cells Materials, USA) current collection layer, were contacted with platinum meshes.

The test C on anode support (AS-C) was aimed to investigate the effect of Mn doping of the YSZ phase in the composite cathode on the cell operation; therefore four cathodes made of LSM30 and Mn-enriched 8YSZ were deposited. The dissolution of Mn oxide into the 8YSZ powder was carried out by heating for 100 h a mixture of 8YSZ powder and Mn-acetate at different temperatures (900, 1000 and 1100 °C). The heat treatment temperature controlled the theoretical amount of Mn oxide dissolved into the 8YSZ phase; the concentrations have been calculated by extrapolating literature data [19] and were expected to be 2.5%, 4.5% and 6.5% moles of Mn oxide per mole of YSZ for 900, 1000 and 1100 °C, respectively. The Mn-enriched powders, as well as the as-received 8YSZ powder, were grinded mechanically in order to decrease the average particle size and were then mixed with LSM30 to prepare the cathode pastes deposited on the anode support. The 2.5% Mn-enriched YSZ was over-grinded to a d_{50} of 0.2 μm unlike the other Mn-YSZ powders, including the as-received 8YSZ, all grinded to 0.3 μm; the as-received LSM30 also had a d_{50} of 0.3 μm. The cell was then sintered at 1050 °C for 1 h; the cathodes, covered with a LSM35 current collection layer, were contacted with gold meshes. Electrical contacting for all anodes supports was achieved with a single Ni mesh, covering the whole anode area opposite to the four cathodes for current collection.

The test on electrolyte support (ES-A) was aimed to investigate the effect of Cr-poisoning in a three-electrode configuration; therefore a metallic interconnect (MIC) sheet (Fe–26Cr stainless steel from *Plansee*) was placed as a source of Cr in proximity of working cathode electrodes. The electrode inks were prepared identically to test AS-B and deposited symmetrically on both sides of the electrolyte support, before sintering for 1 h at 1100 °C and contacting gold meshes to LSM30 current collection layers painted on the electrodes.

2.2. Anode support testing

Cell operation was carried out in a furnace (Rohde, Germany) with a Bentrup TC 505 temperature controller. The cells were placed between two alumina felts and inserted between two metallic flasks (Fig. 2); the test rig was compressed with calibrated springs in order to maintain the metallic meshes under constant pressure on the electrodes. The flasks had central gas inlets in order to feed air to the cathode side and humidified H_2 to the anode side.

There was no sealing between the two compartments so that, during the fuel cell testing, excess H_2 was post-combusted around the cell. Gas flow was adjusted in order to maintain the flame front far from the electrochemical reaction and to minimize H_2O diffusion toward the centre of the support. Typical values for air and H_2 flow were 600 and 250 ml min^{-1}, respectively. Local temperature was monitored through a thermocouple placed near the centre of the support, placed on the air side.

Reduction of the anode supports was conducted at 850 °C while feeding air to the cathode side and H_2 diluted in Ar to the anode

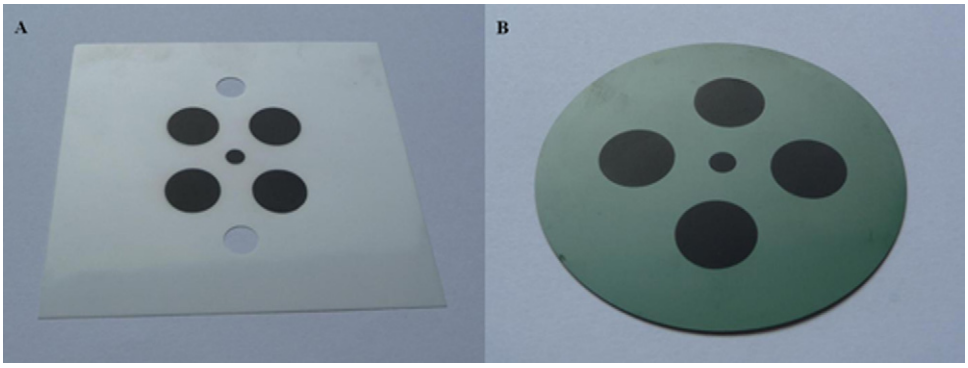

Fig. 1. (A) LSM–YSZ electrodes symmetrically deposited on both sides of 3YSZ electrolyte support. (B) LSM–YSZ cathodes deposited on a Ni-YSZ anode support.

side. The reduction of the NiO took place by a stepwise replacement of argon by hydrogen (H_2 flow varied from 10% to 100%).

The polarization of the cell was done in galvanostatic mode with a four-channel active load built in-house. Measurements were performed in a four-wire configuration. Potential difference, current and temperature data were acquired and stored in a computer through a multi-channel online acquisition device. Electrochemical impedance spectroscopy measurements (EIS) and current–voltage curves were taken with an Eco Chemie Autolab®.

2.3. Electrolyte support testing

Cell operation was performed similarly to anode-supported cells; only air was fed to both sides of the electrolyte, with a flow rate of 250 ml min^{-1}, and the system temperature was kept at 800 °C.

3. Results and discussion

3.1. AS-A, different current densities

After reduction, the four segments have been tested at 850 °C in 3% humidified H_2 and then polarized imposing a current density of 0.3 A cm^{-2} on each of them, thus obtaining EIS and IV curves. After an activation period of 24 h the current density was increased to new constant values on three of the four segments, as shown in Fig. 3; the values are reported in Table 1.

A consensus has been reached explaining the polarization-driven activation, and it has been attributed [20–23] to an increase of oxygen vacancies in the LSM lattice caused by the reduction of Mn ions both because of the current passage and the low oxygen pressure in high overpotential conditions. The test has been continued, over 110 h after activation, in order to compare the effect of different current densities on the behaviour. Fig. 4, which reports the IV curves taken before cell polarization, shows that a difference of about 40 mV is present between the open circuit voltages (OCVs) of the different segments; the difference persists, even if reduced, while passing to higher current densities. This could be related to a inhomogeneous distribution of H_2 and H_2O on the anode support since an insufficient steam content of the fuel (3% in this case), combined with an ill-positioned cell and/or insufficient gas flow to the anode side can lead to unequal diffusion of H_2O at the anode side. To confirm this, Nyquist plots were taken at the beginning of the test and are reported in Fig. 5. While there is a good correspondence in the high frequency part and in the interception with the real axis, it is possible to observe that segments with lower OCV present a lower polarization resistance. Fig. 6 reports the function $\partial Z_{real}/\partial \ln(freq)$ versus frequency (as described by Jensen et al. [24] and successively applied in our laboratory [25,26]), permitting to determine that the process affecting polarization resistance

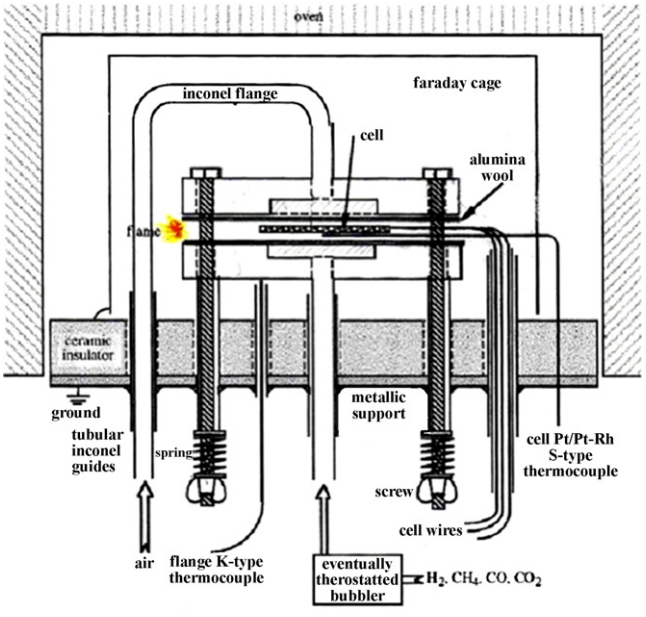

Fig. 2. Test rig used for electrochemical testing. The cells are sandwiched between two alumina felts and placed in the middle of gas feeding flanges. Since no sealing is present, post-combustion of fuel gases takes place around the cell. Local measurement of the temperature is performed by a thermocouple in contact with the cell.

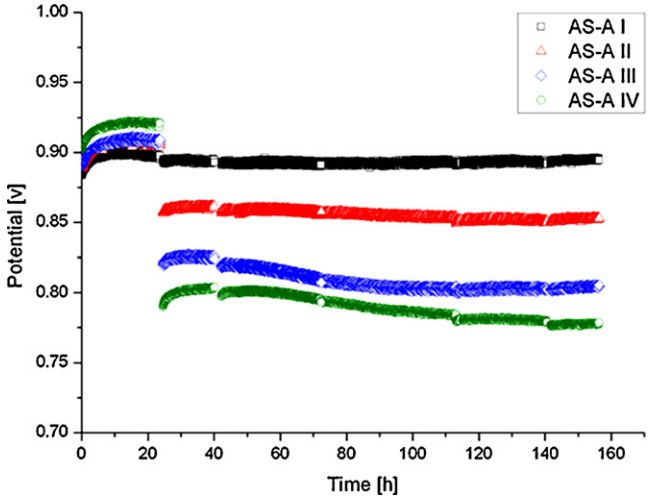

Fig. 3. Operating voltage of AS-A segments. After a 24-h activation period at 0.3 A cm^{-2}, different current densities have been applied to each segment. A second activation appears for higher current density, but also faster degradation.

Table 1
Operating condition for AS-A segments.

Cell	Current density during activation (A cm^{-2})	Current density after activation (A cm^{-2})	Open circuit voltage (mV)
AS-A I	0.30	0.30	1030
AS-A II	0.30	0.45	1050
AS-A III	0.30	0.60	1052
AS-A IV	0.30	0.75	1070

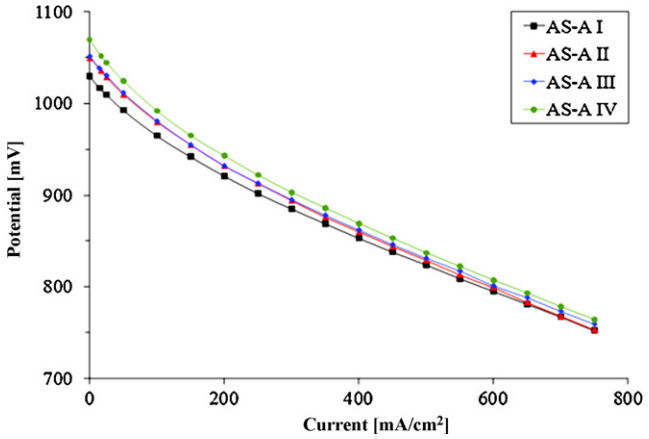

Fig. 4. Current–voltage curves taken on AS-A segments at the beginning of the test. A difference of several 10 mV is present at OCV, attesting a non-homogeneous gas distribution at the fuel side. The difference is reduced while passing current; the general behavior of the segments is very similar.

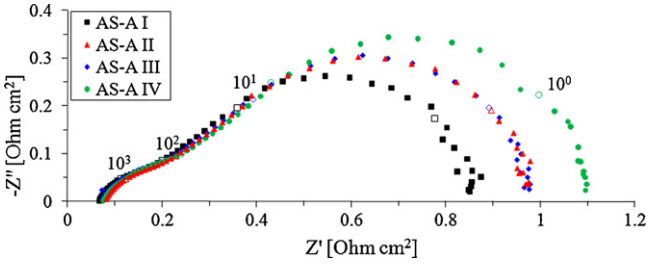

Fig. 5. EIS measurements taken at OCV on AS-A segments at the beginning of the test. The high frequency part of the spectra is reproducible, showing the same intercept with the real axis and the same shape. A difference is present in the low-frequency part of the spectra, showing that segments with lower OCV (Table 1) present lower polarization resistance.

is located at 2–3 Hz. According to the literature [27,28], this frequency is characteristic for gas conversion processes, confirming that the difference in impedance response between the segments is due to a difference in fuel composition at the anode side. In effect, fuel richer in H_2O makes the cell response less sensitive to conversion processes, explaining why the segments with higher OCV show higher polarization resistance.

The behavior in the second part of the test shows more interesting features: a second activation is observed after raising the current density. The phenomenon is more pronounced for higher increases in current density. Moreover, it is possible to observe a relatively fast degradation which saturates after about 100 h. This type of degradation, occurring at the beginning of the tests, has already been observed in our group [5] and in the literature [29] and has been attributed to a microstructural change of the anode support. The present results indicate that the current density has an influence on charge-induced microstructural degradation, as suggested by Presvytes [30].

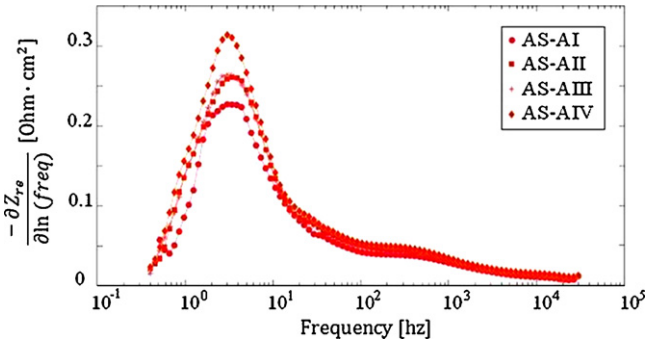

Fig. 6. Frequency analysis of the EIS spectra taken at OCV on AS-A segments at the beginning of the test. The derivation of the real part of impedance permits to identify the characteristic frequency of the processes. The dominating process is conversion at the anode, also responsible for the difference in performance of the segments.

3.2. AS-B, different cathode thickness

The four segments have been tested at 850 °C in 7% humidified H_2 at 0.6 A cm^{-2} for about 1100 h; a failure of gas feeding caused a sudden loss of the integrity of the cell and the stop of the test. With respect to cell AS-A, the increase of the water content in the fuel feed (from 3% to 7%) and a careful positioning of the cell permitted to achieve a uniform gas composition, as testified from the close value range of the segments' OCVs. The same conditions have been used for the results shown in Section 2.3 permitting to achieve very reproducible OCV, as shown in Fig. 11. EIS measurements have been performed at the beginning and after 1000 h of operation. Fig. 7 shows the operating voltage of the four segments during operation; the monolayer cathode (5 μm) shows worse performances than the three other cathodes, which have a similar behavior after activation. This can be explained by the fact that a too thin electrode has its active area limited by the thickness. Micro-modeling based on percolation theory predicts that, in typical SOFC conditions, the reaction extends for 5–10 μm from the electrolyte; the performance of thin electrodes is limited and they benefit from an increase of thickness until this critical thickness is reached [18,31], because of the geometrical extension of the active area. An additional increase in thickness does not extend the active

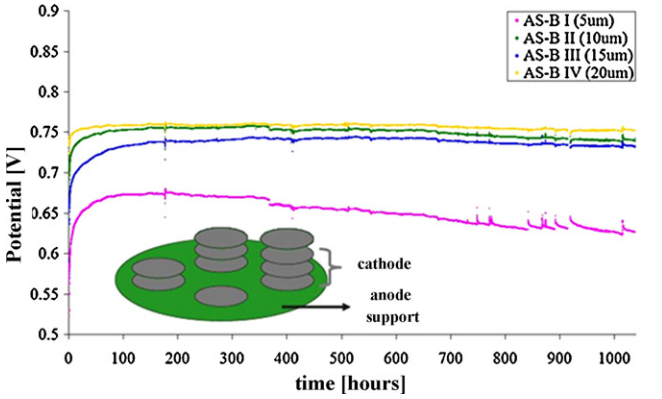

Fig. 7. Operating voltage of AS-B segments. After activation, segment I (5 μm thick) has limited performance while thicker segments have a similar and better performance. Thickness is also related to degradation, with thicker cathodes showing a better stability.

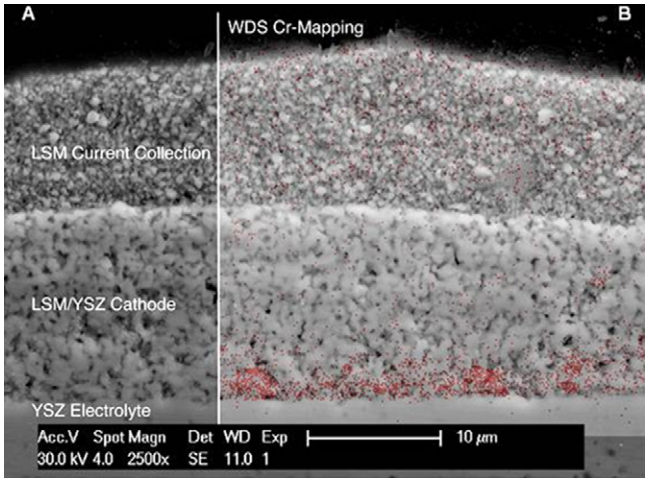

Fig. 8. Image of AS-C III cross-section. (A) SEM image showing the current collection layer and the cathode layer on top of the YSZ electrolyte. (B) Overlapped WDS mapping, showing accumulation of Cr species near the cathode/electrolyte interface.

zone; only the electronic current passes through. The experimental data obtained follow this behavior, showing that an increase in electrode thickness increases the performance but that extra layers above a critical value do not cause further improvement.

Degradation was found to be acceptable for the 4-layer cathode (~0.9%/1000 h). These results show a clear trend, increasing with decreasing thickness. The degradation rate has been estimated to about ~1.5%/1000 h for the 3-layer cathode, ~2.2%/1000 h for the 2-layer cathode and ~6%/1000 h for the monolayer cathode. This could indicate the presence of a contaminant, like traces of Cr into the active cathode layer stemming from the tubing elements and test flanges (made of Inconel 602 alloy). The increased number of actives sites for oxygen reduction is suggested to delay performance decrease for cathodes with increased thickness [10]. Short-term re-activation caused by the interruption of the current has been found, followed by a rapid decay, as it has already been reported in literature in the case of Cr-poisoning [11,13].

EIS measurements explained why cell AS-B III had an initial performance worse than cells II and IV which evolve towards a similar performance with time. It seems that at the beginning of the test, the ohmic resistance, found at the high frequency intercept of the spectrum with the real axis, is higher for segment AS-B III (about 0.5 $\Omega\,cm^2$) than for the other three segments; the latter show all three a similar value of about 0.2 $\Omega\,cm^2$. During operation at high temperature and under the pressure of the metallic flanges, the contacting meshes increase their adhesion to the electrodes and improve the electrical contact. At the end of the test, all ohmic resistances were found to be close to a value of 0.12 $\Omega\,cm^2$. The comparison between the spectra at different operation times shows that the polarization resistance has decreased for all cells, due to the activation process taking place in the first tens of hours of operation (this is masked for cell III by the variation in ohmic resistance).

Cr-contamination of cathode electrodes was revealed by scanning electron microscopy (SEM), performed on an XLF-30 SEM from *FEI*, coupled to energy dispersive X-ray spectroscopy (EDS), done with a EDS detector and software from *Oxford Instruments*. Accumulations of Cr near the cathode/electrolyte interface was confirmed examining the cross-section of the segment AS-C III by wavelength-dispersive X-ray spectroscopy (WDS), realized on a *JEOL* 8200 electron probe, as illustrated in Fig. 8.

3.3. AS-C, Mn-doped YSZ in cathode composite

The four segments have been tested at 850 °C in 7% humidified H_2 at 0.6 A cm^{-2} for about 800 h.

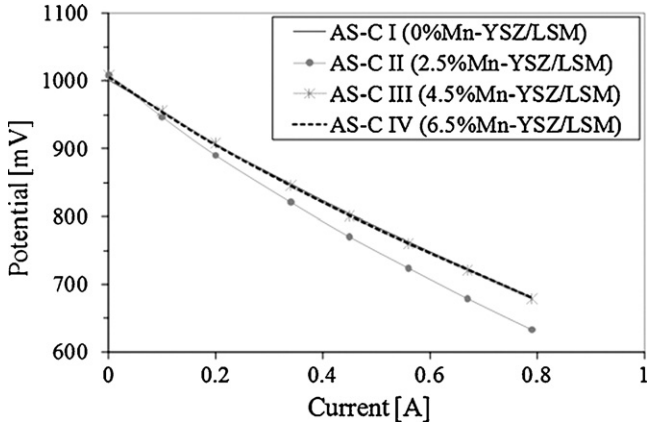

Fig. 9. Current–voltage curves taken on AS-C segments at the beginning of the test. The curves are overlapped for segments with the same microstructure while AS-C II, containing over-grinded YSZ particles, shows the same OCV but poorer performances.

Initial characterization showed a good reproducibility for the three cells with the same microstructure while the cell with finer YSZ (the 2.5% Mn-enriched) had poorer performances (Fig. 9).

EIS spectra have been taken at different times, temperatures, gas compositions and current densities. The fuel composition was obtained by mixing H_2 and Ar in different proportion. This gas flux was bubbled through a bottle of de-mineralized water kept at constant temperature to control the amount of gaseous water. Testing conditions are reported in Table 2.

The analysis of EIS data permitted to identify the characteristic frequencies of the semi-circles and the sensitivity of the different processes from the operation variables, according to the analyses present in literature [24,27,28]. Table 3 reported the characteristic frequencies, sensitivities and the process that has been attributed to each semicircle. This preliminary analysis allowed investigating what processes changed during aging and the effect of the composition on the degradation.

3.4. ES-A, Cr-poisoning

As chromium stemming from test-rig-components (Inconel 602 alloy) was found in test AS-B as air-side contaminant, an additional Cr-source (Fe–26Cr stainless steel) was placed in proximity of the working cathode electrode in this electrolyte supported test for accelerated Cr-poisoning. Taniguchi et al. performed a pioneering work on Cr-poisoning and reported the cathode polarization increase to be in correlation with the intensity of chromium at the cathode/electrolyte interface; Cr-vapors originated from Inconel 600 alloy in their study [12]. In this work, the potential of the symmetrical cell polarized under 200 mA cm^{-2} and that of the working cathode were monitored, their evolution with time is shown in Fig. 10.

Table 2
Measurement conditions for EIS investigation on AS-C segments.

Temperature	Fuel composition	Bias current densities (A cm^{-2})
850 °C	93% H_2, 7% H_2O, 0% Ar	0.0, 0.3, 0.6
	65% H_2, 7% H_2O, 28% Ar	0.0, 0.3, 0.6
	65% H_2, 5% H_2O, 30% Ar	0.0, 0.3, 0.6
800 °C	93% H_2, 7% H_2O, 0% Ar	0.0, 0.3
	65% H_2, 7% H_2O, 28% Ar	0.0, 0.3
	65% H_2, 5% H_2O, 30% Ar	0.0, 0.3
750 °C	93% H_2, 7% H_2O, 0% Ar	0.0, 0.3
	65% H_2, 7% H_2O, 28% Ar	0.0, 0.3
	65% H_2, 5% H_2O, 30% Ar	0.0, 0.3

Table 3
Principal contributions of the polarization resistance. The sensitivity to operating variables and the characteristic frequencies are reported.

Frequency	Sensitivity	Process
10 Hz	Fuel composition (high)	Conversion, anode
30 Hz (750 °C) 70 Hz (800 °C) 200 Hz (850 °C)	Current density (high), temperature (high)	Dissociative adsorption, cathode
700 Hz (750 °C) 1000 Hz (800 °C) 2000 Hz (850 °C)	Current density (high), temperature (high), fuel composition (low)	Charge transfer, anode
200 Hz	Fuel composition (very low)	Diffusion, anode (not clear, small signal)

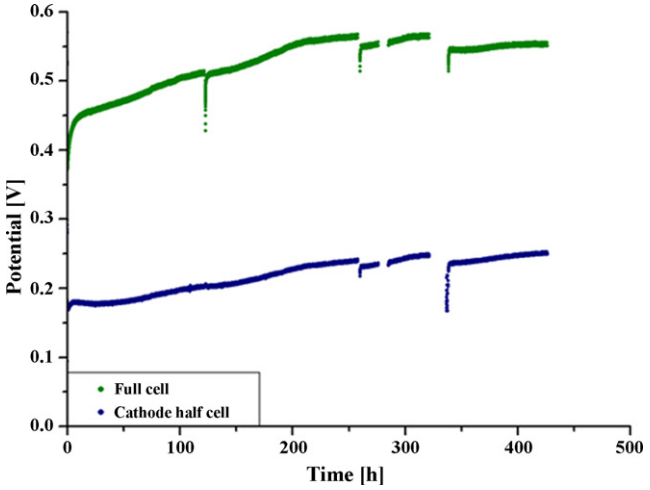

Fig. 10. Evolution of cell and electrode potentials with time under a current load of 200 mA cm^{-2}.

The cell potential increases with time and is well correlated to the cathode (abr. for working cathode electrode) performance decrease upon Cr-poisoning. Transients in operation, i.e. switching of the current load for EIS measurements, induce voltage recovery as mentioned above which is known for Cr-polluted cathodes [10,11,13]. The cathode degradation is severe, as the half-cell potential increases almost 50% during 400 h of operation, indicating Cr to block oxygen access and reduction in the thin cathode (5 μm thickness). The central reference electrode allowed separating working and counter electrode half-cell contributions. In fact, the high frequency part of the spectra contained a measurement artifact, probably due to a too high contact resistance of the reference electrode; however, after eliminating the data points obtained above ~10^4 Hz, it was possible to obtain a proper separation, where the sum of the two half-cell contributions equals the total impedance of the symmetrical cell, as show in Fig. 11, thus validating the concept of multiple cathode testing. A solution has been found for lowering the contact resistance, namely through

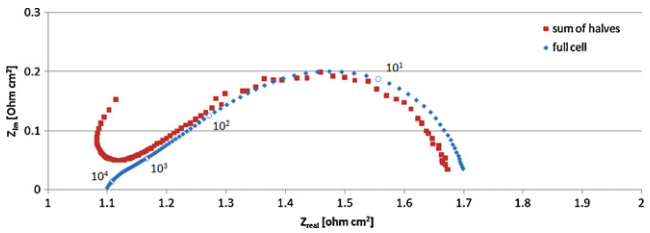

Fig. 11. Validation of the separation by a reference electrode. The point-by-point summation of the impedances measured on the two half cells is compared to the impedance of the full cell measured in a four-electrode configuration.

the contacting of the reference electrode with additional gold paste, avoiding the presence of the artifact.

The second symmetrical cell, kept as reference and not polarized, did not show a noticeable degradation. The behavior of these two cells, tested rigorously in the same conditions and on the same support, indicates that current load is a key parameter in Cr-poisoning. Moreover, this test has proven the feasibility of accelerated testing of Cr-poisoning.

4. Conclusions

Segmented cell testing has been proven to be an original, effective strategy to achieve better reproducibility for SOFC measurements by avoiding the inevitable fluctuation for a series of successively run tests. Moreover, simultaneous testing increased *n*-fold the data output per experiment, implying a considerable economy of time.

The present work has shown that, in a segmented cell configuration, investigations on several variables like current density, electrode composition, electrode thickness, and gas phase composition can be performed maintaining the flexibility of single button-cell configuration.

Moreover, it was possible to observe that typical artifacts affecting SOFC measurements (e.g. change in ohmic contact in the first part of the operation) can be easily identified by comparison between segments and taken into account.

A further development can be the introduction of a segmented anode-supported cell in a sealed test rig, to avoid H_2 diffusion and therefore a possible non homogenous fuel distribution at the anode side.

Acknowledgments

The authors want to thank the SOF-CH, the Swiss SOFC Consortium, co-financed by the Swiss Federal Office of Energy (SFOE), contract number 152210 and Swisselectric Research. The SFOE is also acknowledged for funding the AccelenT project, contract number 153569.

We would like to express gratitude to our industrial partners SOFCpower©-HTceramix©for material supply and use of equipment.

F. Bussy from the Institute of Mineralogy and Geochemistry/Faculty of Geosciences and Environment/University of Lausanne is gratefully acknowledged for WDS-analyses.

References

[1] S.P. Jiang, J. Mater. Sci. 38 (2003) (2003) 3775–3782.
[2] A. Faes, A. Hessler-Wyser, D. Presvytes, C.G. Vayenas, J. Van herle, Fuel Cells 9 (6) (2009) 841–851.
[3] H. Tu, U. Stimming, J. Power Sources 127 (1–2) (2004) 284–293.
[4] S.P. Jiang, W. Wang, Solid State Ionics 176 (13–14) (2005) 1185–1191.

[5] P. Tanasini, M. Cannarozzo, P. Costamagna, A. Faes, J. Van Herle, A. Hessler-Wyser, C. Comninellis, Fuel Cells 9 (5) (2009) 740–752.
[6] H. Oppolzer, Analytics for Materials. Siemens-Review Special - R&D, 1996. Fall 1996, pp. 5–7.
[7] M. Chen, A.N. Grundy, B. Hallstedt, L.J. Gauckler, Comput. Coupling Phase Diagrams Thermochem. 30 (2006) 489–500.
[8] H. Yokokawa, S. Yamauchi, M. Takafumi, Thermochim. Acta 245 (1994) (1994) 45–55.
[9] A. Mitterdorfer, L.J. Gauckler, Solid State Ionics 111 (3–4) (1998) 185–218.
[10] E. Konysheva, J. Mertens, H. Penkalla, L. Singheiser, K. Hilpert, J. Electrochem. Soc. 154 (12) (2007) 271–278.
[11] S.P.S. Badwal, R. Deller, K. Foger, Y. Ramprakash, J.P. Zhang, Solid State Ionics 99 (3–4) (1997) 297–310.
[12] S.M.K. Taniguchi, H. Kawamura, T. Yasuo, Y. Akiyama, Y. Miyake, T. Saitoh, J. Power Sources 55 (1) (1995) 73–79.
[13] Y. Matsuzaki, I. Yasuda, Solid State Ionics 132 (3–4) (2000) 271–278.
[14] H. Yokokawa, T. Horita, N. Sakai, K. Yamaji, M.E. Brito, Y.P. Xiong, H. Kishimoto, Solid State Ionics 177 (35–36) (2006) 3193–3198.
[15] M. Hattori, Y. Takeda, J.-H. Lee, S. Ohara, K. Mukai, T. Fukui, S. Takahashi, Y. Sakaki, A. Nakanishi, J. Power Sources 131 (1–2) (2004) 247–250.
[16] J. Van Herle, R. Vasquez, J. Eur. Ceram. Soc. 24 (6) (2004) 1177–1180.
[17] C. Haering, A. Roosen, H. Schichl, Solid State Ionics 176 (3–4) (2005) 253–259.
[18] P. Costamagna, P. Costa, V. Antonucci, Electrochim. Acta 43 (3–4) (1998) 375–394.
[19] T. Kawada, N. Sakai, H. Yokokawa, M. Dokiya, Solid State Ionics 53–56 (Part 1) (1992) 418–425.
[20] E. Siebert, A. Hammouche, M. Kleitz, Electrochim. Acta 40 (11) (1995) 1741–1753.
[21] F.S. Baumann, J. Fleig, M. Konuma, U. Starke, H.U. Habermeier, J. Maier, J. Electrochem. Soc. 152 (10) (2005) A2074–A2079.
[22] X.J. Chen, K.A. Khor, S.H. Chan, Solid State Ionics 167 (2004) (2003) 379–387.
[23] W. Wang, S.P. Jiang, J. Solid State Electrochem. (8) (2004) 914–922.
[24] S.H. Jensen, A. Hauch, P.V. Hendriksen, M. Mogensen, N. Bonanos, T. Jacobsen, J. Electrochem. Soc. 154 (12) (2007) B1325–B1330.
[25] Z. Wuillemin, A. Nakajo, A. Müller, A.J. Schüler, S. Diethelm, J. Van Herle, D. Favrat, ECS Trans. 25 (2 Part 1) (2009) 457–466.
[26] Z. Wuillemin, PhD Thesis - Experimental and modeling investigations on local performance and local degradation in solid oxide fuel cells, EPFL, Lausanne, 2009.
[27] R. Barfod, M. Mogensen, T. Klemensoe, A. Hagen, Y.L. Liu, P.V. Hendriksen, Proc. SOFC IX 1 (2005) (2005) 503–513.
[28] M.J. Jørgensen, M. Mogensen, J. Electrochem. Soc. 148 (5) (2001) A433–A442.
[29] A. Hagen, Y.L. Liu, R. Barfod, P.V. Hendriksen, J. Electrochem. Soc. 155 (10) (2008) B1047–B1052.
[30] D. Presvytes, Solid Oxide Fuel Cells: Triode Operation, Mathematical Modelling and Temperature Programmed Desorption Investigation, University of Patras, 2009.
[31] P. Costamagna, P. Costa, E. Arato, Electrochem. Acta 43 (8) (1997) 967–972.